General Disclaimer

One or more of the Following Statements may affect this Document
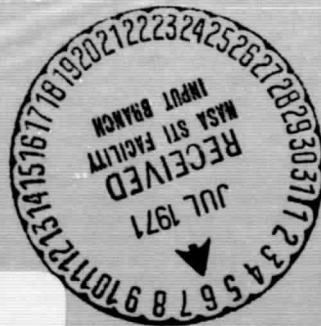
- This document has been reproduced from the best copy furnished by the organizational source. It is being released in the interest of making available as much information as possible.

- This document may contain data, which exceeds the sheet parameters. It was furnished in this condition by the organizational source and is the best copy available.

- This document may contain tone-on-tone or color graphs, charts and/or pictures, which have been reproduced in black and white.

- This document is paginated as submitted by the original source.

- Portions of this document are not fully legible due to the historical nature of some of the material. However, it is the best reproduction available from the original submission.

U.S. DEPARTMENT OF COMMERCE
OFFICE OF TELECOMMUNICATIONS
Institute for Telecommunication Sciences
BOULDER, COLORADO

L-31028

Phase and Amplitude Scintillations of Microwave
Signals Over an Elevated Atmospheric Path

M. C. Thompson, Jr. , H. B. Janes, L. E. Wood, &

Dean Smith

Phase and Amplitude Scintillations of Microwave
Signals C ʳer an Elevated Atmospheric Path
M. C. Thompson, Jr. , H. B. Janes, L. E. Wood, &
Dean Smith

PHASE AND AMPLITUDE SCINTILLATIONS OF MICROWAVE
SIGNALS OVER AN ELEVATED ATMOSPHERIC PATH

M. C. Thompson, Jr. , H. B. Janes, L. E. Wood, & D. Smith

Institute for Telecommunication Sciences, Boulder, Colo.

Background

A technique has been proposed to obtain global surveys of atmospheric density profiles by means of a set of co-orbital earth satellites [Lusignan, et al. , 1969]. The method involves measurements of phase delays in microwave signals propagated between pairs of satellites, so arranged that the signal passes through the atmosphere along a part of its path.

A basic factor in the success of this technique is the influence of random atmospheric variability (turbulence) on signal phase and amplitude. These signal properties are also involved in the bandwidth required in the satellite terminal equipment. In addition, other atmospheric propagation effects, notably fading, could have a significant effect on the overall effectiveness of the system. The phenomenon of principal concern in this respect is the very deep (e. g. , > 50 dB) fades associated with certain types of refractive index gradients known to occur.

The objectives of the experiment reported here were:

1. to obtain a basic statistical description of phase and fading characteristics using a fixed propagation path chosen to simulate certain

aspects of the satellite-to-satellite configuration; and,

2. in conjunction with the fixed path measurements, to obtain simultaneous measurements of atmospheric index structure near the propagation path.

Location

Since only the portions of the atmosphere above about 2.5 km are to be probed in the proposed system, a path was sought with two high terminals and a maximum surface clearance. Chiefly because of logistic factors (e. g. , roads, shelter, power, etc.) the path selected was between Mt. Haleakala, Maui, Hawaii, and Mauna Loa, Hawaii. The terminal elevations are 3025 m and 3300 m, respectively, and the path length is 150 km.

Figures 1 and 2 show the locations and profile, including the half-power beam widths of the antennas.

Radio Measurements

Three converging paths were instrumented at frequencies near 10 GHz. A single terminal at Mauna Loa Observatory was equipped with a 2-m diameter parabolic dish having a 1.2^{o} beam width. The Haleakala terminal was equipped with three 1.25-m diameter dishes having 1.8^{o} beams. These antennas were spaced along a line perpendicular to the nominal direction of propagation with 10 m between the first and second, and 100 m between the first and third. This permitted

measurement of the variability of phase-front orientation.

The quantities recorded were:

1. Amplitudes of signals from each of the three antennas with a dynamic range of from 20 to 50 dB, precision of 0.5 dB, and frequency response from 0 to 30 Hz.

2. Phase variability on each of the three paths with unlimited dynamic range, 0.5 degree resolution (at the X-band frequency), and response from 0 to 30 Hz.

3. Phase differences between the 10 m spaced antennas and between the 100 m pair, with same recording ranges, etc., as in (2). A description of the phase measurement system is given in Appendix IV (attached).

Atmospheric Measurements

A Piper "Aztec" aircraft was equipped with a microwave refractometer and flown in the vicinity of the path to obtain refractive index structure and statistics. Because of the locations of the beam intersections (Fig. 2), flights were concentrated between about 2 and 4 km elevation.

Operations and Results

The radio signals were observed continuously from 0800 hours June 15 through 0500 hours June 29. Aircraft flights were made on 23 occasions during this period.

During the first four days of the run signal amplitudes were generally variable but without the characteristic "V"-shaped appearance associated with the very deep fades. In the next four days the deep fades occurred a large fraction of the time. Figure 3 shows an example of these two types of activity.

Initially, the plan was to obtain index profiles at two locations along the path plus a record of horizontal index variability along the path; the latter data would provide estimates of the index structure parameter C_n which might correlate with signal variability [Tatarski, 1961; Porcello, 1970].

At the onset of deep fading, it was decided to modify the flight plan to obtain as many vertical sections (profiles) as feasible along the path. These would show the horizontal extent of the vertical index features that might be related to the deep fading.

As an approximate preliminary description of the fading, the data have been divided into four groups in terms of the amplitude variability within 30-min periods.

The groups are defined as follows:

Type A: < 5 dB peak to peak fading range.

Type B: > 5 dB peak to peak fading range.

Type C: > 5 dB with from 1 to 5 "V"-shaped fades of > 15 dB.

Type D: > 5 dB with over 5 "V"-shaped fades > 15 dB.

This classification is used in Figs. 4 and 5, together with the corresponding flight patterns, to summarize the amplitude variability with respect to time and time of day.

Figures 6, 7, and 8 show examples of index profiles obtained during Flights 4 and 12, the same periods used for the fading samples in Fig. 3. Two kinds of profiles were obtained from the refractometer data. The "low-pass" output of the refractometer was used to produce the familiar profiles of N versus height. At the same time, a "band-pass" output provides a profile of small-scale N variability as a function of height. Both low-pass and band-pass profiles are shown for Flight 4 in Fig. 6. They are plotted separately for Flight 12 in Figs. 7 and 8. Because of the relatively low angle at which the plane ascends and descends (about 6°), the record is subject to horizontal index variations to an appreciable degree. Thus one should not assume that the resulting plots represent the true vertical structure of index.

A description and the results of the analysis of the refractometer data from level flights along the propagation path is given in Appendix I (attached). The results consist of values of the refractive index structure parameter, C_n, computed from level flight segments. A complete

set of refractive index profile graphs is included as a part of this report in separate Appendix II.

Signal Data Analysis

From the 14-day measurement period, detailed statistical analysis was performed on a sample of signal phase, phase difference, and amplitude data taken from each of the 23 aircraft flight periods. (In the results, note that "sample number" and "flight number" are synonymous, and that there was no flight 6.)

Each of the signal data samples is 40 min in length except for 7 samples which were shortened to avoid phase discontinuities. The discontinuities were caused by deep fading in 5 cases and by equipment trouble in the other 2 cases. Frequent fading discontinuities precluded statistical analysis of the phase data from samples 8, 11, and 12.

With the exceptions noted above, each signal sample was analyzed to produce the cumulative distribution and power spectrum of each of the phase and amplitude variables, and cross-correlation and coherency functions of appropriate pairs of variables. The original analog magnetic tape recordings were digitized at the rate of 12.5 points per variable per second. Of these, every tenth point was used (without smoothing) in the cross-correlation computations. For the power spectrum and coherency computations, the data were smoothed by averaging non-overlapping groups of 10 points in order to minimize aliasing effects. The

cumulative distributions were also computed from smoothed data.

The results of the signal data analyses are included as a part of this report in separate Appendix III. They consist of the following:

1. Computer printouts of:

a. Cumulative distributions of phase and amplitude data at each of the 3 antenna locations on Haleakala, and of 2 phase-difference records (from the 10-m path separation of antennas 1, 2, and the 100-m separation of antennas 1, 3). These include histograms, standard deviations, 10%, 50%, and 90% levels and (for amplitude) the mean level.

b. Cross-correlation functions of the phase data for 10 and 100 meter path separations, and of the corresponding amplitude data.

c. Power spectra and coherency functions for the same data mentioned in b above, and power spectra of the two phase-difference variables.

Examples of the computer tabulations are given in Figs. 9 through 11.

2. Computer-generated graphs of:

a. Power spectra of phase, phase difference, and amplitude.

b. Coherency functions of phase and amplitude.

c. Cumulative distributions of amplitude.

Examples are given in Figs. 12 through 16.

With regard to units, the amplitude data are expressed in terms

of decibels relative to an arbitrary reference level common to all the samples recorded on a given path. Thus it is possible to compare amplitude levels from sample to sample on the same path (as is done in the amplitude distribution graphs), but amplitude levels on different paths should not be compared.

The phase data are all expressed in phase degrees at 9. 6 GHz Because phase continuity was not maintained from sample to sample, the phase levels listed in the distributions are simply relative to the sample mean.

These restrictions on comparisons of phase and amplitude levels do not, of course, apply to comparisons of phase and amplitude variability and covariability (i. e. , standard deviation, interdecile range, cross-correlation coefficient, power spectral density, and coherency). The only caution here would be with regard to the amplitude on path 2, which was recorded with a detector having a smaller dynamic range than those used on paths 1 and 3. Hence, the amplitude variability statistics from path 2 are less accurate than those from the other two paths.

Acknowledgment

Haleakala terminal, the facilities of the University of Hawaii Observatory were made available through the courtesy of Dr. John Jeffries, Director, Geophysical Institute. The other terminal was located at the Mauna Loa Observatory of the ESSA Environmental Research Laboratories, operated by the Atmospheric Physics and Chemistry Laboratory, Dr. H. Weickmann, Director.

List of Figures

References

1. Lusignan, B., G. Madrell, A. Morrison, J. Pomalaza, and S. Unger, "Sensing the earth's atmosphere with occultation satellites," Proc. IEEE 57, No. 4, April 1969.

2. Thompson, M. C., Jr., and M. J. Vetter, "Single path phase measuring system for three-centimeter radio waves," Rev. Sci. Instr. 29, No. 2, Feb. 1958.

3. Tatarski, V. L., Wave Propagation in a Turbulent Medium, McGraw-Hill Book Co., Inc., New York, 1961.

4. Porcello, L. J., "Turbulence-induced phase errors in synthetic-aperture radars, IEEE Trans. Aerospace Electron. Sys. AES-6, No. 5, Sept. 1970.
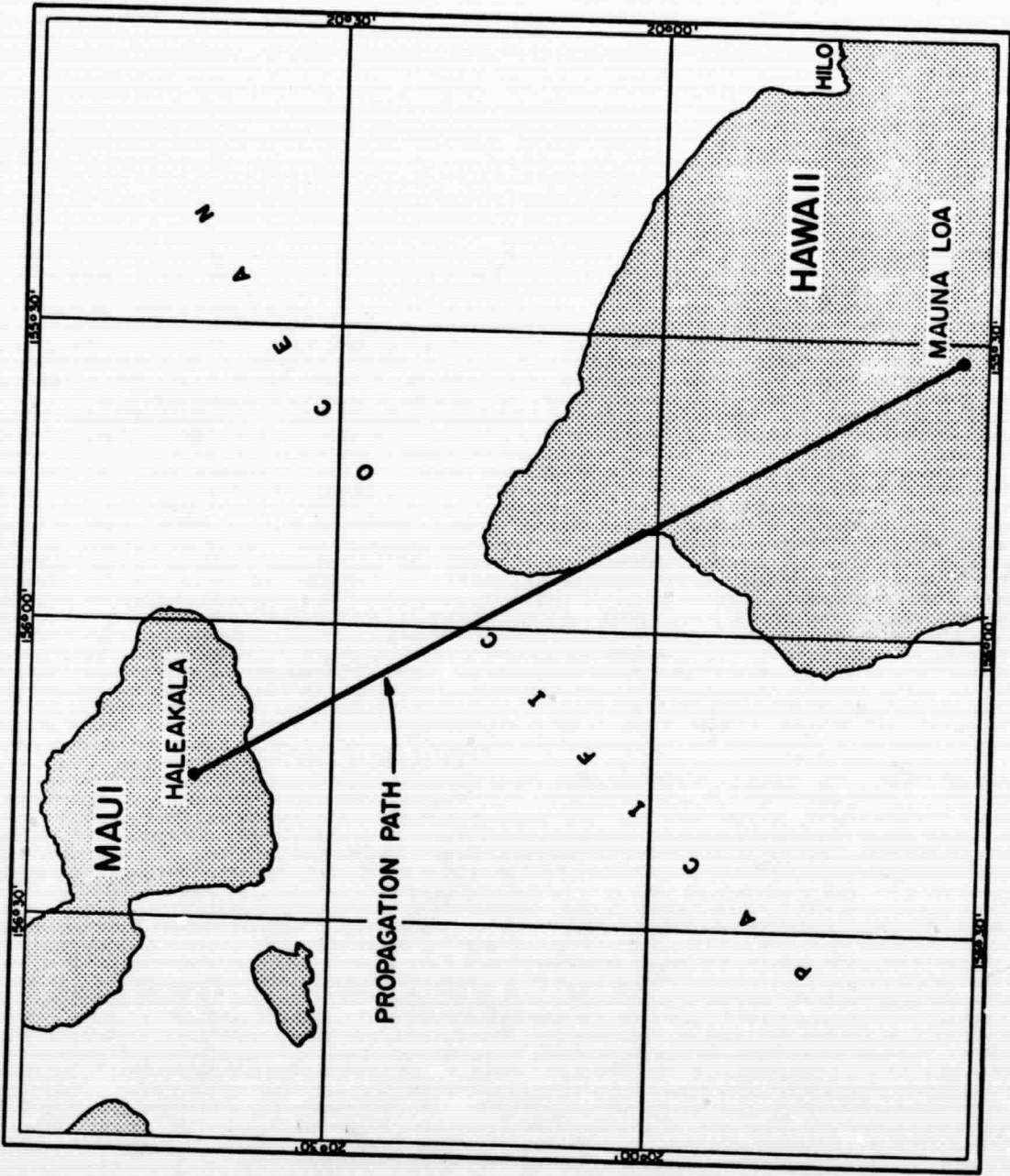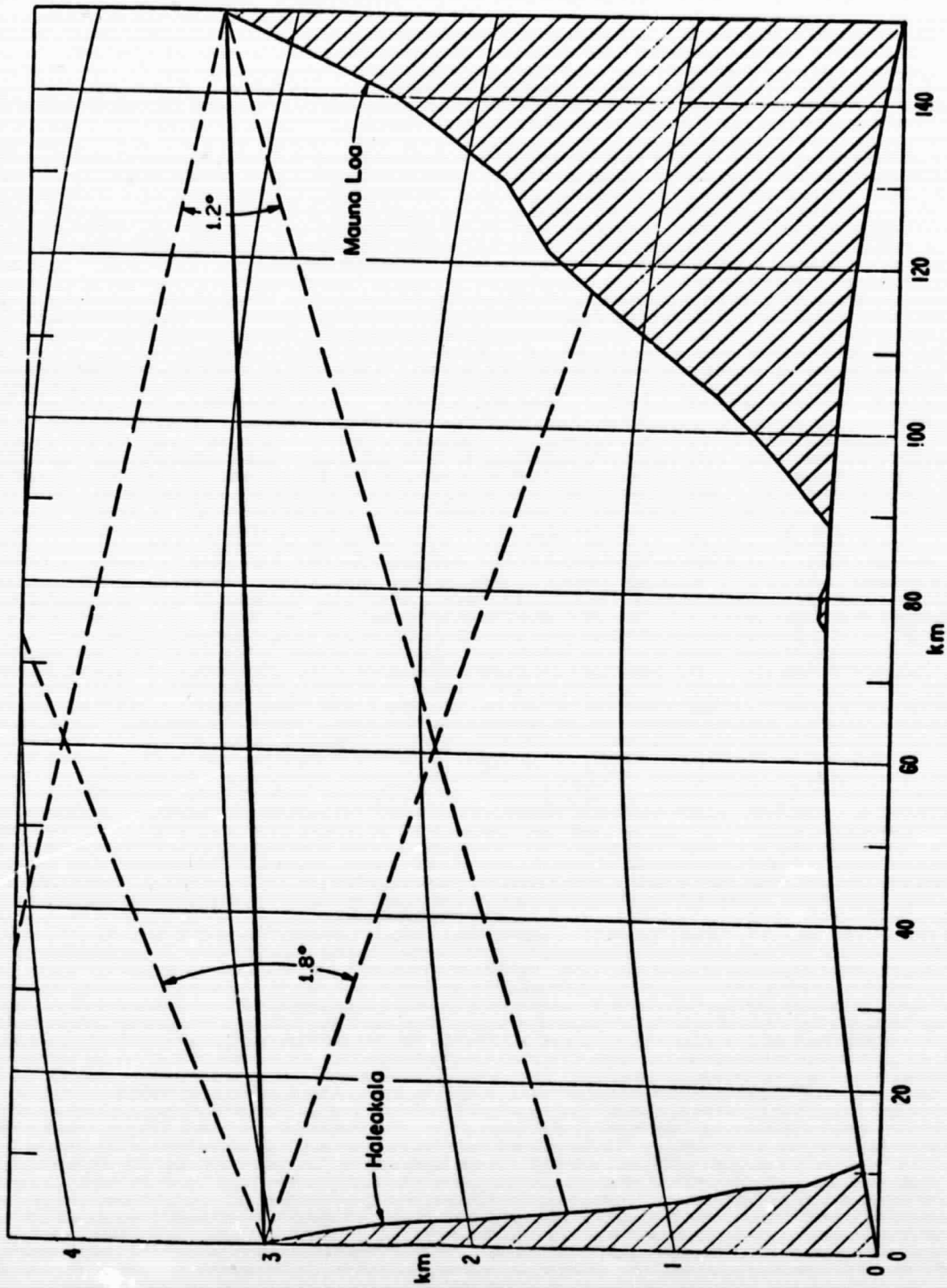
Fig. 1. Map of propagation path.

Fig. 2. Vertical profile of propagation path. The dashed lines indicate the half-power beamwidth of the antennas.

SIGNAL FADING ON SIMULATED SATELLITE OCCULTATION PATH
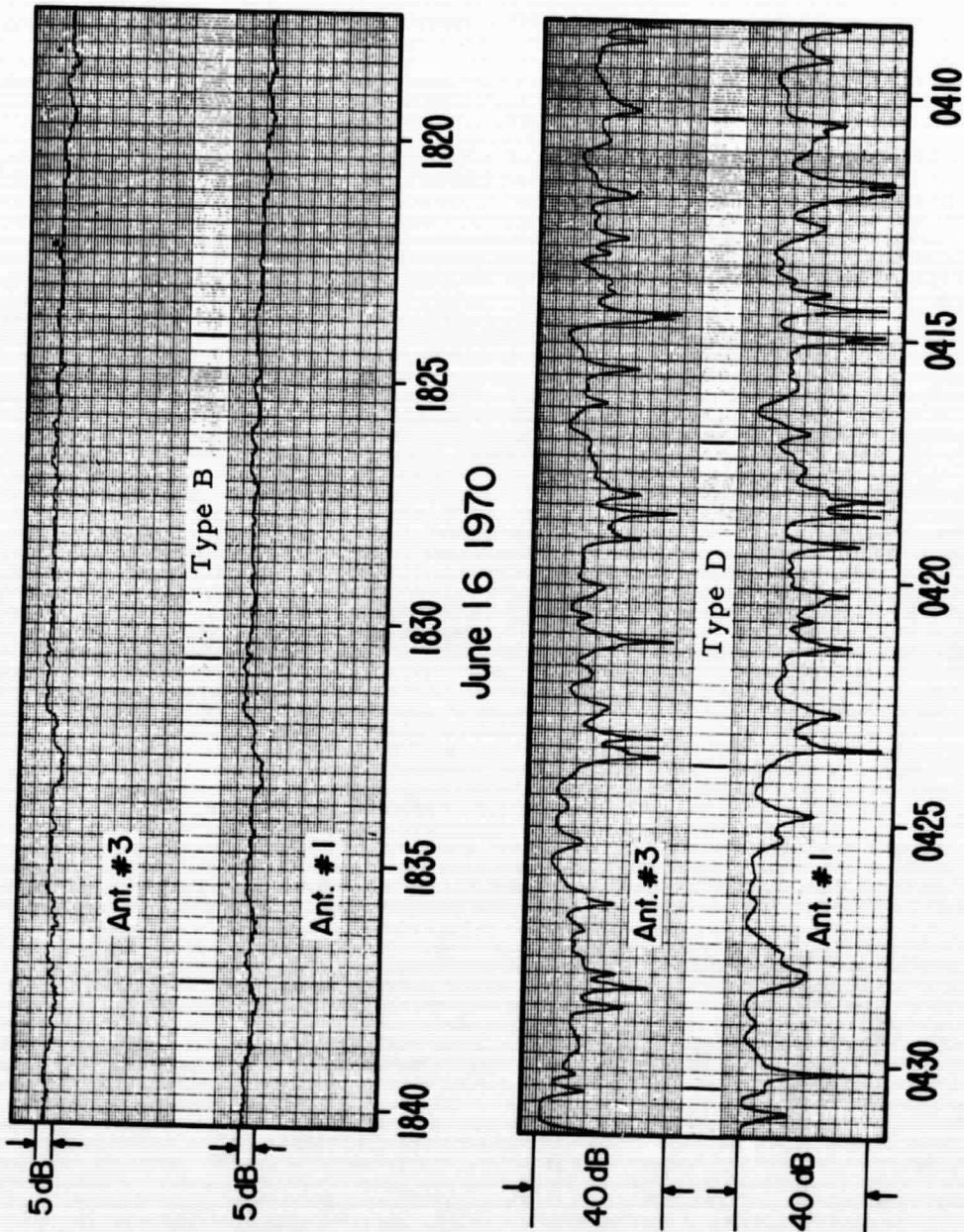## Horizontal Antenna Separation at Haleakala: 100m

June 16 1970

June 22, 1970

Fig. 3

SUMMARY OF FADING DATA
HAWAII, JUNE 1970 9.6 GHz

FADING TYPES
(in terms of peak-to-peak fading range within a 30 min. period)

A: < 5dB
B: > 5dB
C: > 5dB with 1 to 5 "V" shaped fades > 15 dB
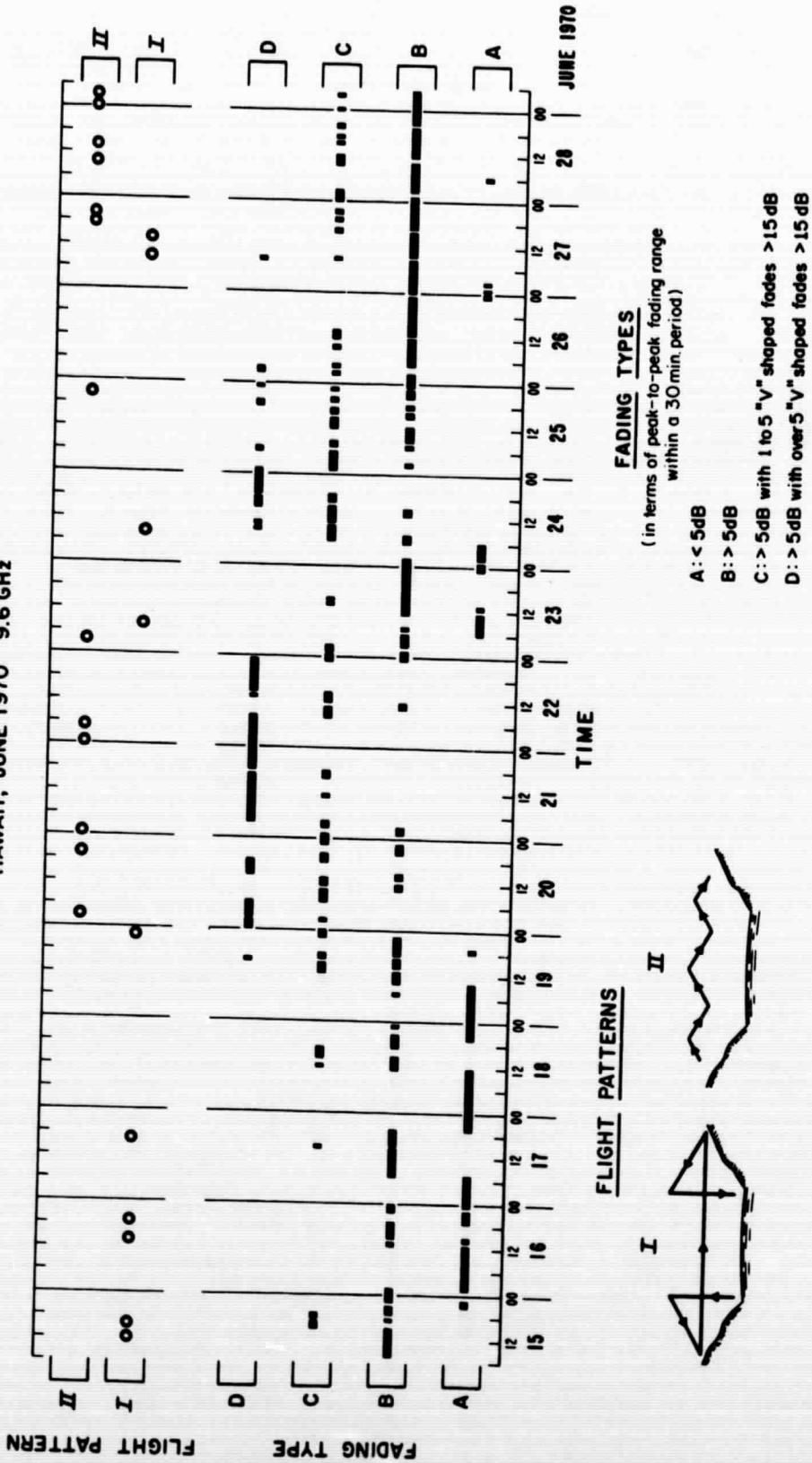D: > 5dB with over 5 "V" shaped fades > 15 dB
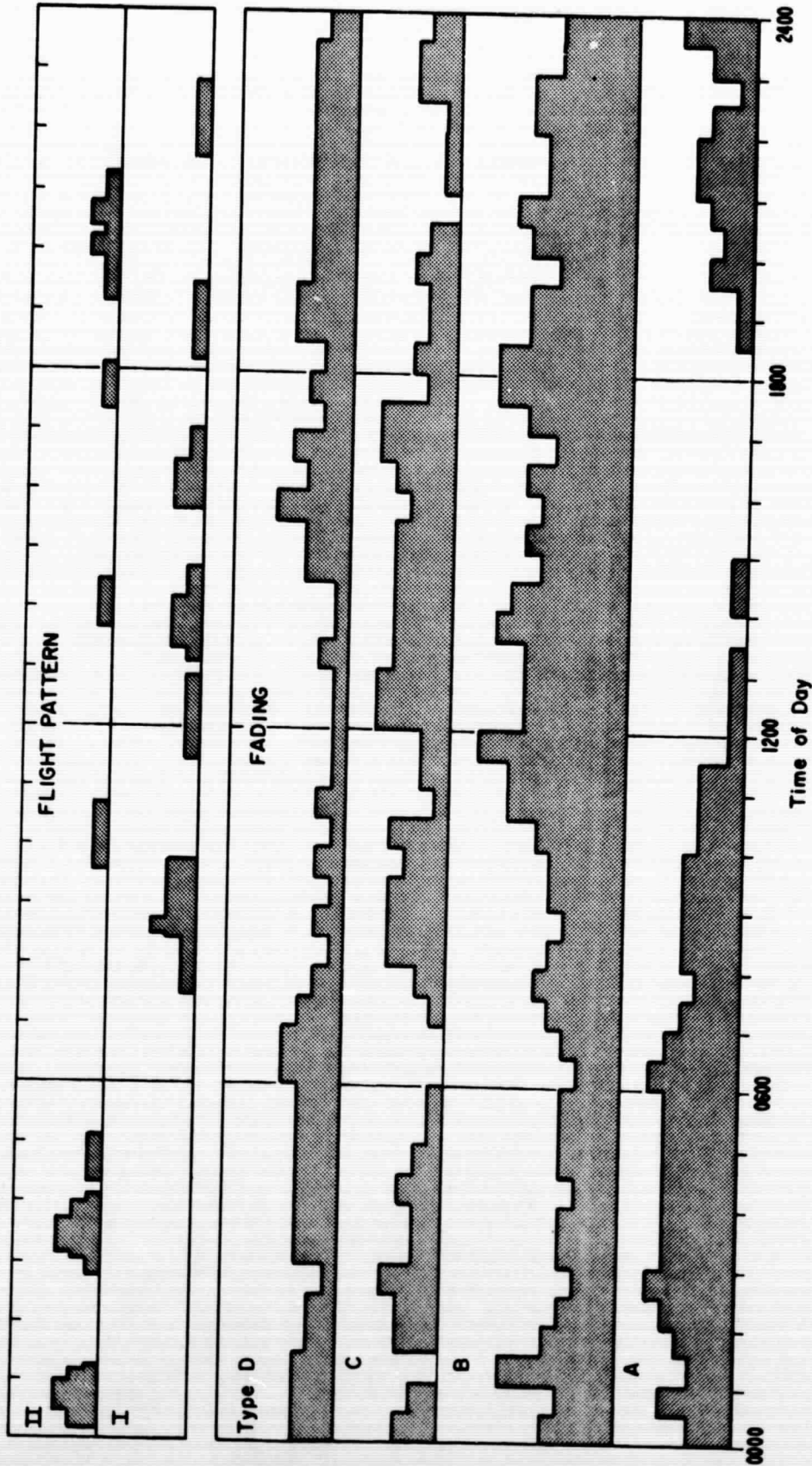
FLIGHT PATTERNS

Fig. 4.

- 14 -

Fig. 5. Distribution of fading occurrences and refractometer flights with time of day. See Fig. 4 for explanation of fading types and flight patterns.
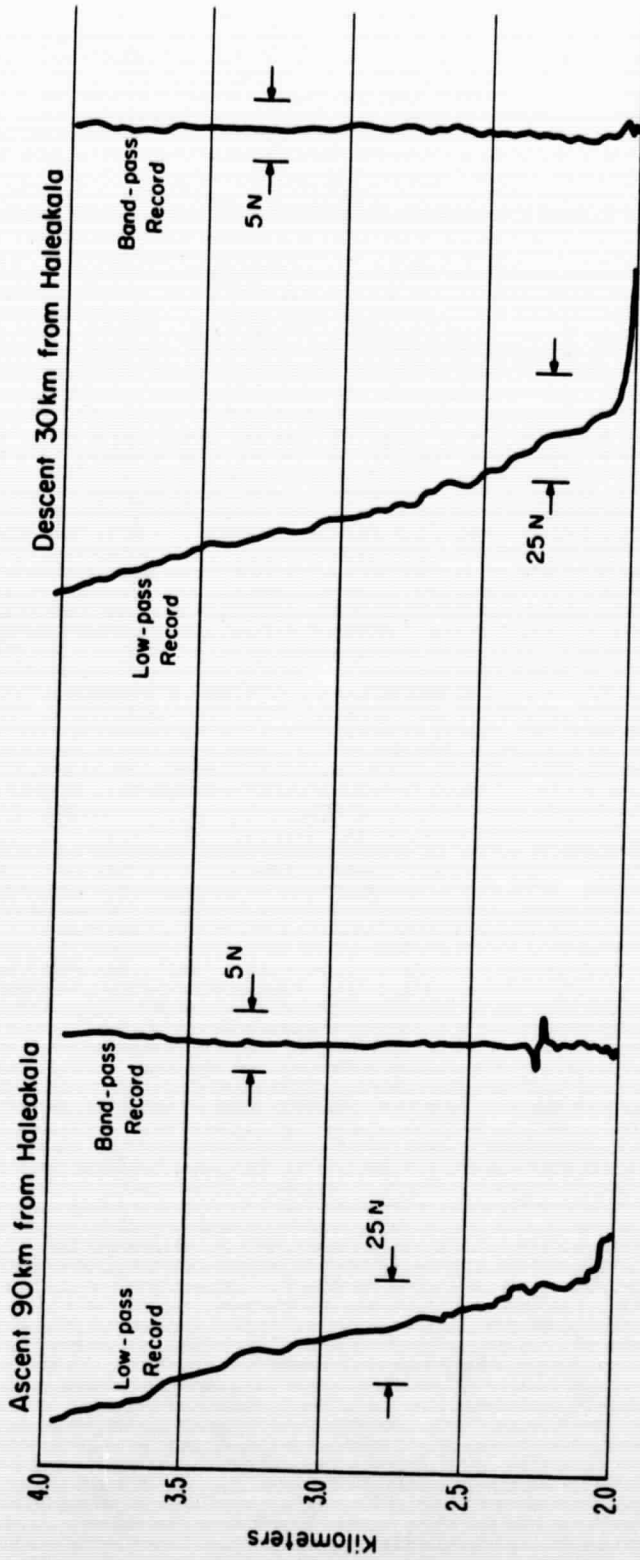
- 15 -

Fig. 6. Examples of refractive index profile data. Profiles from both low-pass and band-pass recordings are shown for Flight 4.

Fig. 7. Example of refractive index profile data. Four profiles from low-pass recordings made during Flight 12.
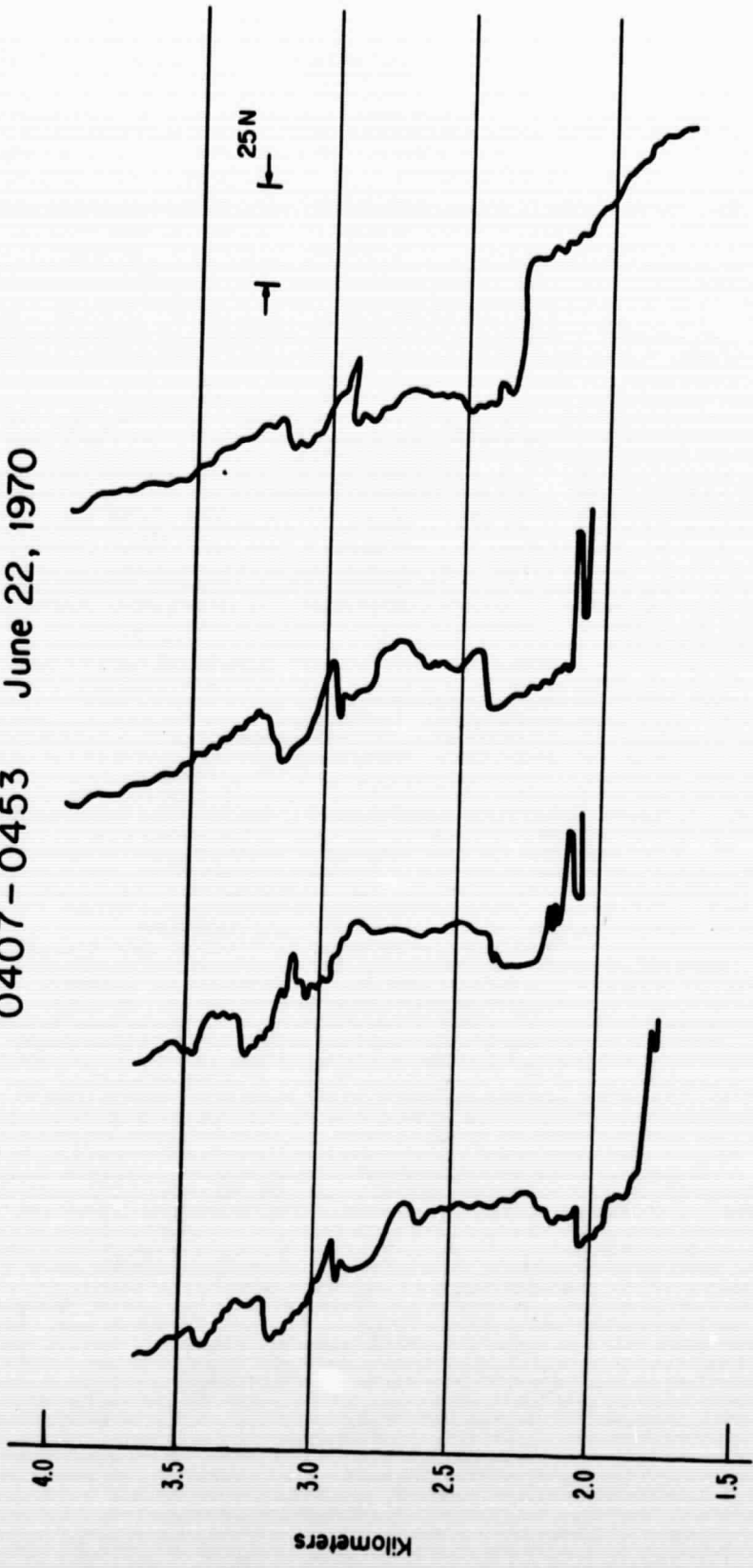
Fig. 8. Example of refractive index profile data. Four profiles from band-pass recordings made during Flight 12.
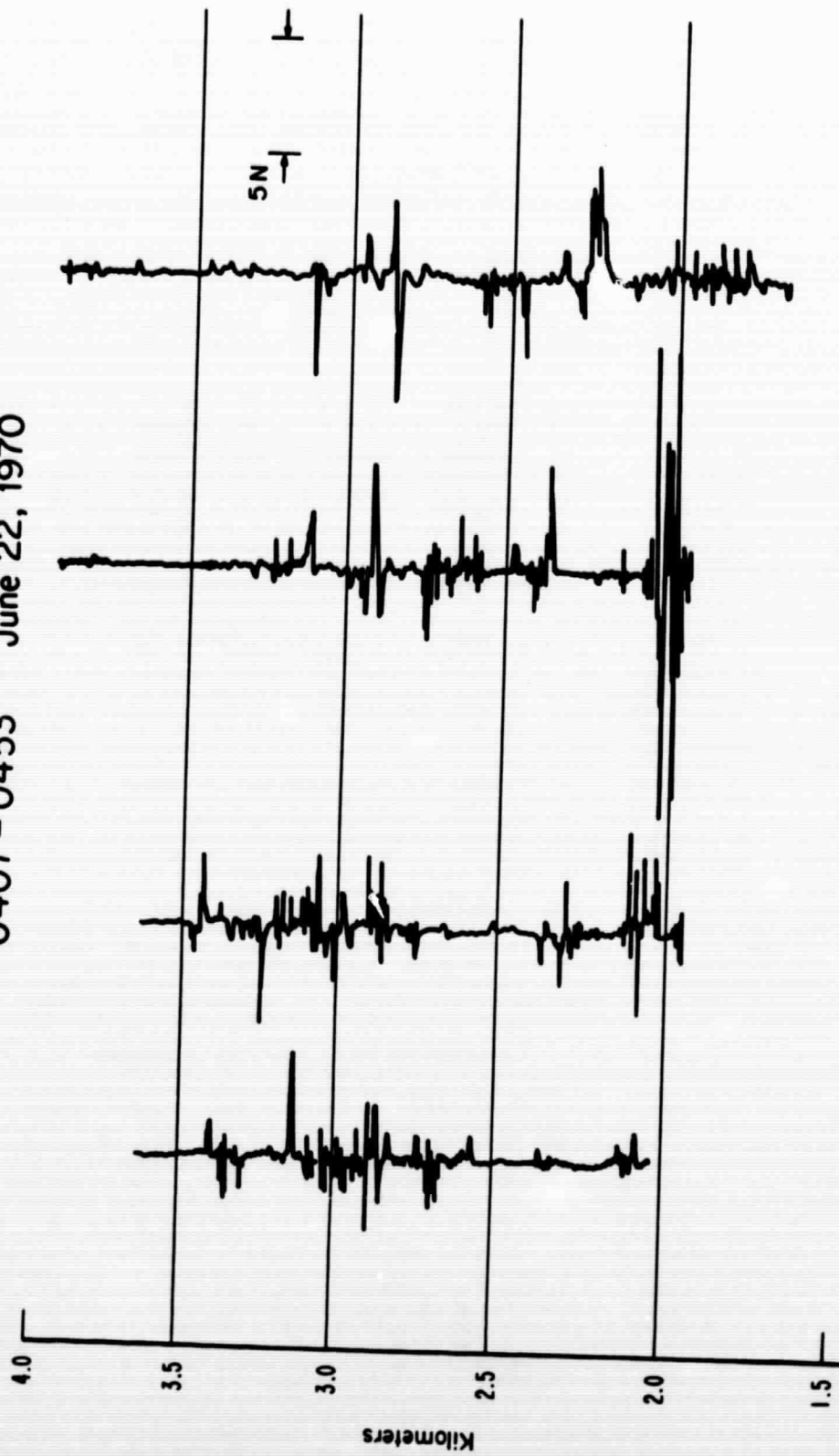
FLIGHT 12   HAWAII
0407-0453   June 22, 1970

5N

Kilometers

4.0   3.5   3.0   2.5   2.0   1.5

OCCULTATION EXPERIMENT   DISTRIBUTION ANALYSIS   SAMPLE NO. 4   TIME: 1840 - 1920 JUNE 16, 1970
VARIABLE: = AMPLITUDE AT ANTENNA 1   DATA COUNT = 3044   UNITS: DECIBELS   SAMPLING INTERVAL 0.8 SECONDS

PERCENT AT LEVEL

LEVEL	DISTRIBUTION COUNT AT LEVEL	≥ LEVEL	PERCENT ≥ LEVEL	0 · · · 25 · · · 50 · · ·
3.52+001	0	0	0.0	X
3.47+001	12	12	0.4	X
3.43+001	46	58	1.9	XXX
3.38+001	74	132	4.3	XXX
3.33+001	86	218	7.2	XXXX
3.28+001	183	401	13.2	XXXXXX
3.23+001	237	638	21.0	XXXXXXXX
3.18+001	252	890	29.2	XXXXXXXX
3.13+001	259	1149	37.7	XXXXXXXXX
3.09+001	305	1454	47.8	XXXXXXXXXXX
3.04+001	339	1793	58.9	XXXXXXXXXXXX
2.99+001	312	2105	69.2	XXXXXXXXXXXX
2.94+001	358	2463	80.9	XXXXXXXXXXXXXX
2.89+001	275	2738	89.9	XXXXXXXXXXXXX
2.84+001	118	2856	93.8	XXXXX
2.79+001	92	2948	96.8	XXXX
2.75+001	66	3014	99.0	XXX
2.70+001	26	3040	99.9	XX
2.65+001	3	3043	103.0	X
2.60+001	1	3044	100.0	X

MEAN: 3.086+001
STANDARD DEVIATION: 1.619+010
10 % LEVEL: 3.31+001
50 % LEVEL: 3.08+001
90 % LEVEL: 2.89+001

(LEVELS SHOWN ABOVE ARE RELATIVE TO AN ARBITRARY REFERENCE COMMON TO ALL SAMPLES OF THIS VARIABLE)

HEADER IN   12040   3511   70030

Fig. 9. Example of signal amplitude distribution analysis included in separate Appendix III.

- 19 -

Fig. 11. Example of cross-spectrum analysis of signal amplitude data included in separate Appendix III.

MAXIMUM CORRELATION AT A POSITIVE LAG MEANS VARIATIONS OCCURRED FIRST AT X.

PLOT SYMBOLS: + (-) MEANS CORRELATION COEFFICIENTS FOR POSITIVE (NEGATIVE) LAG
               B MEANS BOTH COEFFICIENTS ARE APPROXIMATELY EQUAL

THESE ANSWERS ARE FROM ORIGINAL DATA   SPACED BY 10 POINTS
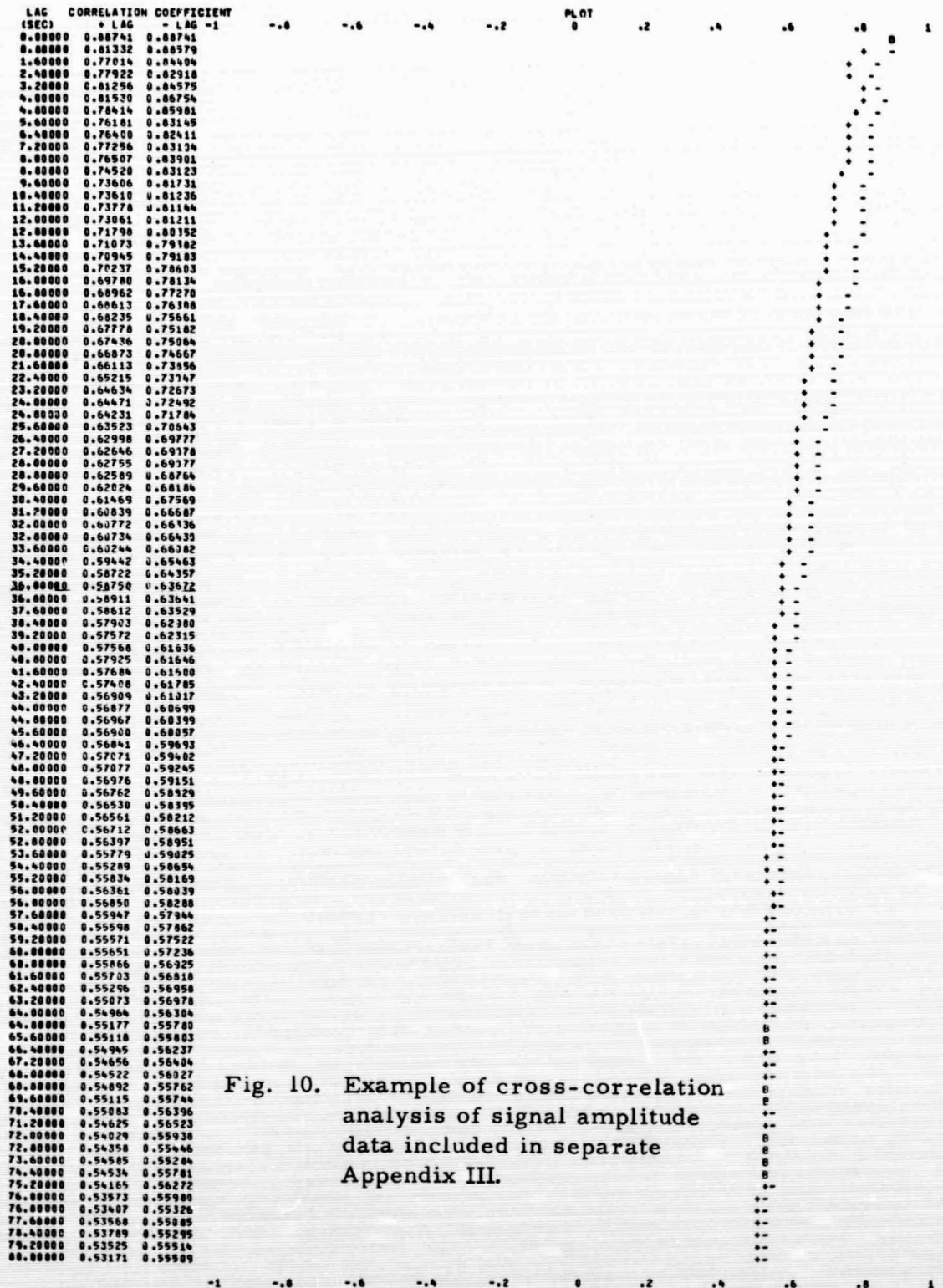VARIANCE (X) = 3.04744+000 VARIANCE (Y) = 2.60894+000 COVARINC = 2.50220+000

LAG	CORRELATION COEFFICIENT		PLOT
(SEC)	+ LAG	- LAG	-1 -.8 -.6 -.4 -.2 0 .2 .4 .6 .8 1
0.00000	0.88741	0.88741	
0.80000	0.81332	0.88579	
1.60000	0.77014	0.84404	
2.40000	0.77922	0.82918	
3.20000	0.81256	0.84575	
4.00000	0.81530	0.86754	
4.80000	0.78414	0.85981	
5.60000	0.76181	0.83145	
6.40000	0.76400	0.82411	
7.20000	0.77256	0.83134	
8.00000	0.76507	0.83901	
8.80000	0.74520	0.83123	
9.60000	0.73606	0.81731	
10.40000	0.73610	0.81236	
11.20000	0.73778	0.81144	
12.00000	0.73061	0.81211	
12.80000	0.71798	0.80152	
13.60000	0.71073	0.79182	
14.40000	0.70945	0.79183	
15.20000	0.70237	0.78603	
16.00000	0.69780	0.78134	
16.80000	0.68962	0.77270	
17.60000	0.68613	0.76388	
18.40000	0.68235	0.75661	
19.20000	0.67778	0.75182	
20.00000	0.67436	0.75064	
20.80000	0.66873	0.74667	
21.60000	0.66113	0.73856	
22.40000	0.65215	0.73147	
23.20000	0.64634	0.72673	
24.00000	0.64471	3.72492	
24.80000	0.64231	0.71784	
25.60000	0.63523	0.70643	
26.40000	0.62998	0.69777	
27.20000	0.62646	0.69178	
28.00000	0.62755	0.69177	
28.80000	0.62589	0.68764	
29.60000	0.62024	0.68184	
30.40000	0.61469	0.67569	
31.20000	0.60839	0.66687	
32.00000	0.60772	0.66136	
32.80000	0.60734	0.66430	
33.60000	0.60244	0.66382	
34.40000	0.59442	0.65463	
35.20000	0.58722	0.64357	
36.00000	0.58750	0.63672	
36.80000	0.58911	0.63641	
37.60000	0.58612	0.63529	
38.40000	0.57903	0.62380	
39.20000	0.57572	0.62315	
40.00000	0.57568	0.61636	
40.80000	0.57925	0.61646	
41.60000	0.57684	0.61500	
42.40000	0.57408	0.61785	
43.20000	0.56909	0.61317	
44.00000	0.56877	0.60699	
44.80000	0.56967	0.60399	
45.60000	0.56900	0.60857	
46.40000	0.56841	0.59693	
47.20000	0.57071	0.59402	
48.00000	0.57077	0.59245	
48.80000	0.56976	0.59151	
49.60000	0.56762	0.58929	
50.40000	0.56530	0.58395	
51.20000	0.56561	0.58212	
52.00000	0.56712	0.58663	
52.80000	0.56397	0.58951	
53.60000	0.55779	0.59025	
54.40000	0.55289	0.58654	
55.20000	0.55834	0.58169	
56.00000	0.56361	0.58039	
56.80000	0.56850	0.58288	
57.60000	0.55947	0.57944	
58.40000	0.55598	0.57862	
59.20000	0.55571	0.57522	
60.00000	0.55651	0.57236	
60.80000	0.55866	0.56925	
61.60000	0.55703	0.56818	
62.40000	0.55296	0.56958	
63.20000	0.55073	0.56978	
64.00000	0.54964	0.56304	
64.80000	0.55177	0.55780	
65.60000	0.55118	0.55803	
66.40000	0.54945	0.56237	
67.20000	0.54656	0.56404	
68.00000	0.54522	0.56027	
68.80000	0.54492	0.55762	
69.60000	0.55115	0.55744	
70.40000	0.55063	0.56396	
71.20000	0.54625	0.56523	
72.00000	0.54029	0.55938	
72.80000	0.54358	0.55446	
73.60000	0.54585	0.55284	
74.40000	0.54534	0.55781	
75.20000	0.54165	0.56272	
76.00000	0.53573	0.55900	
76.80000	0.53407	0.55326	
77.60000	0.53568	0.55085	
78.40000	0.53789	0.55295	
79.20000	0.53525	0.55514	
80.00000	0.53171	0.55509	

Fig. 10. Example of cross-correlation analysis of signal amplitude data included in separate Appendix III.

-1   -.8   -.6   -.4   -.2   0   .2   .4   .6   .8   1

I-92294

OCCULTATION EXPERIMENT

Cumulative Distribution of Amplitude at Antenna 1

▲ Sample 1, 1155-12.35   June 15, 1970
x Sample 2, 1558-1619   June 15, 1970
⊙ Sample 3, 1330-1410   June 16, 1970
+ Sample 4, 1840-1920   June 16, 1970

Percentage of data exceeding the ordinate
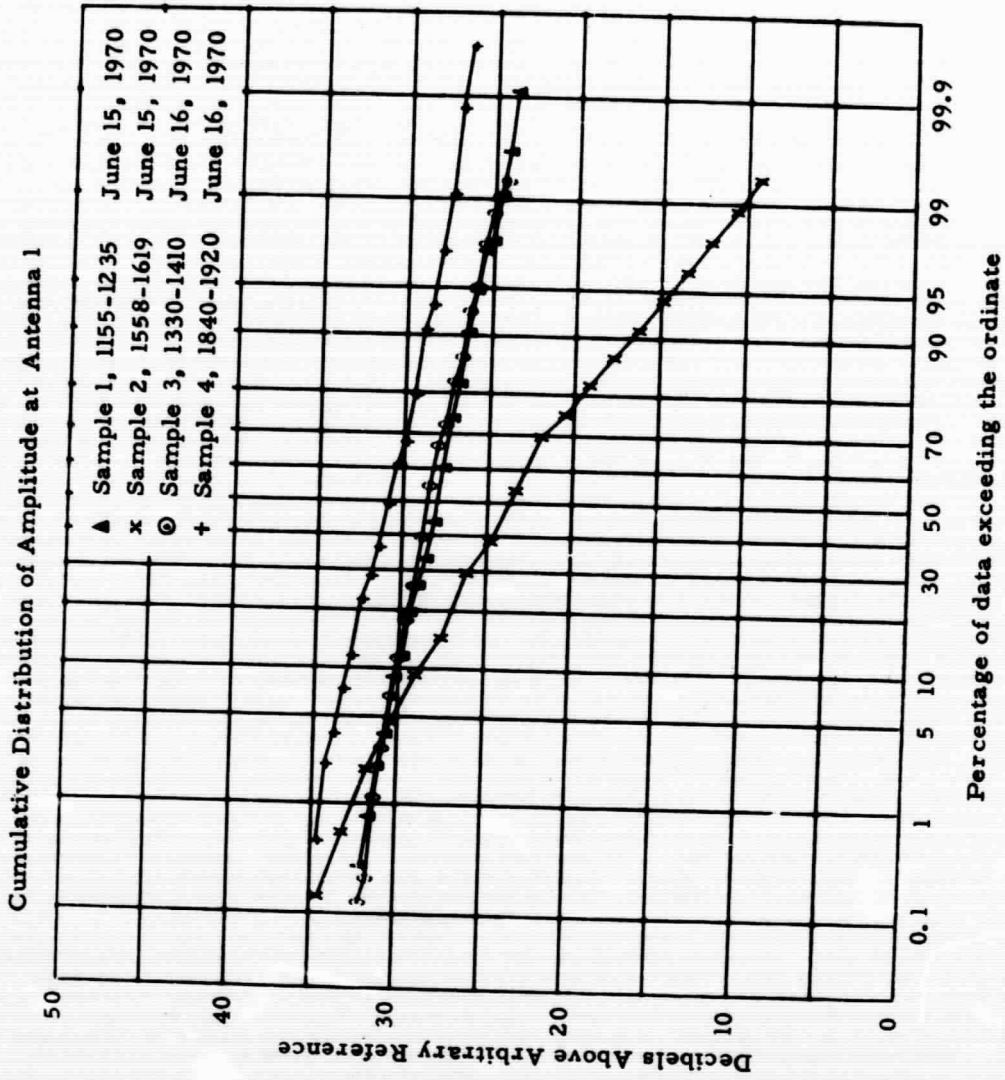
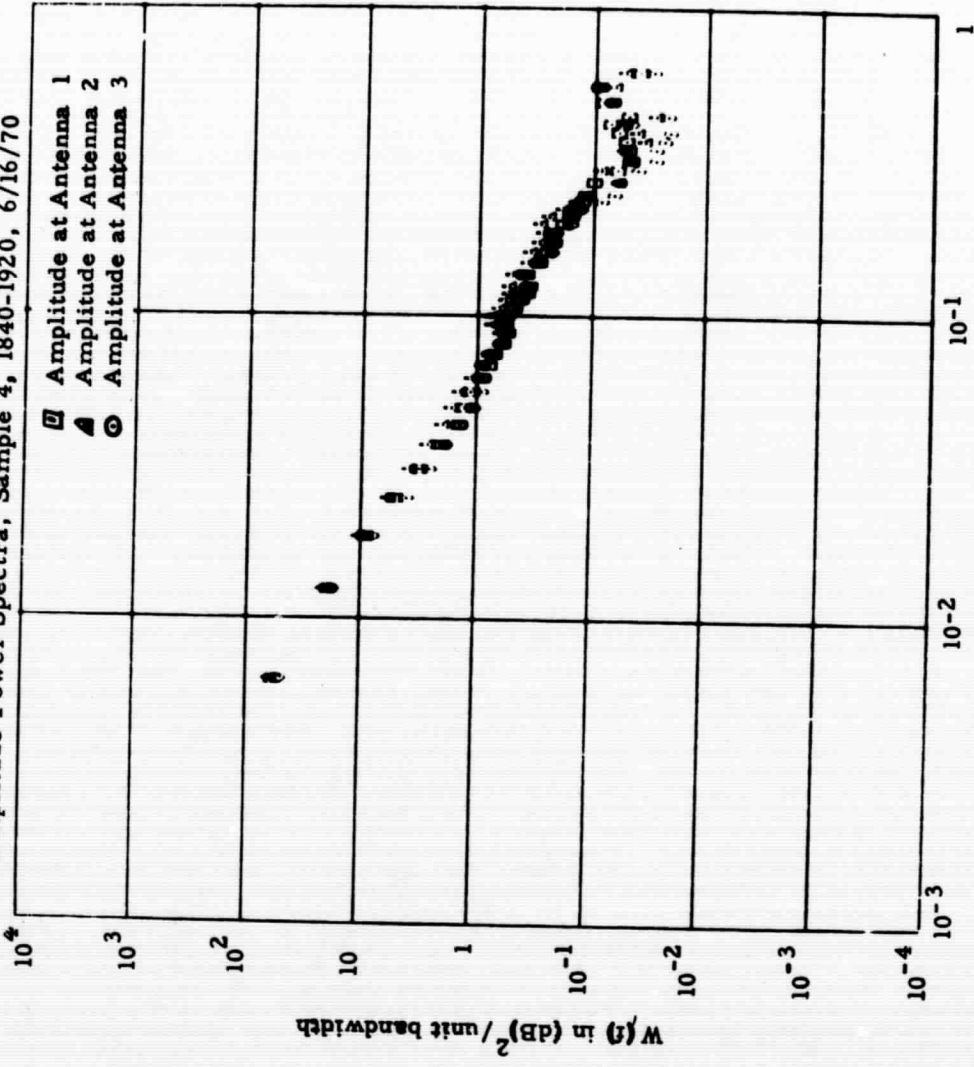Decibels Above Arbitrary Reference

Fig. 12

OCCULTATION EXPERIMENT

Amplitude Power Spectra, Sample 4, 1840-1920, 6/16/70

Fig. 13

- 23 -

OCCULTATION EXPERIMENT

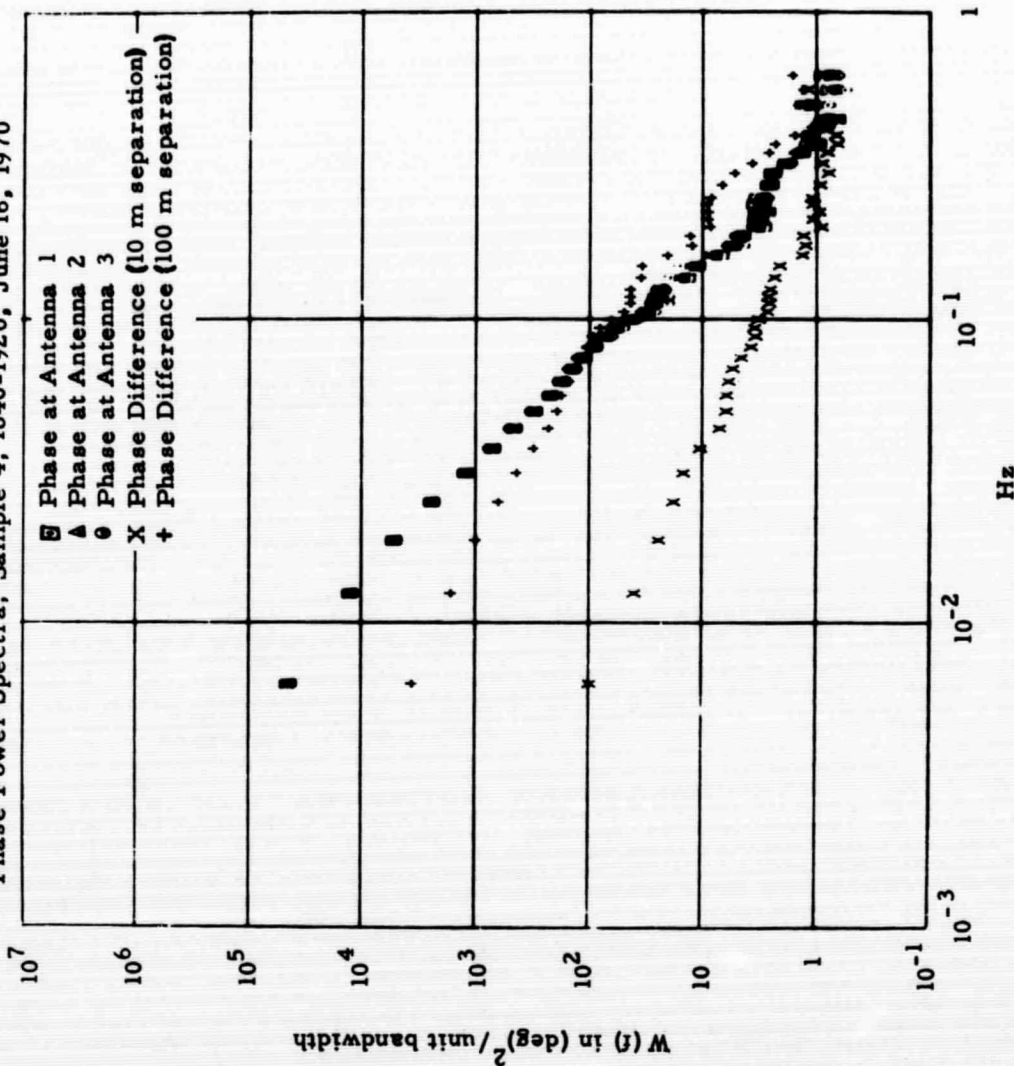Phase Power Spectra, Sample 4, 1840-1920, June 16, 1970

Fig. 14

OCCULTATION EXPERIMENT

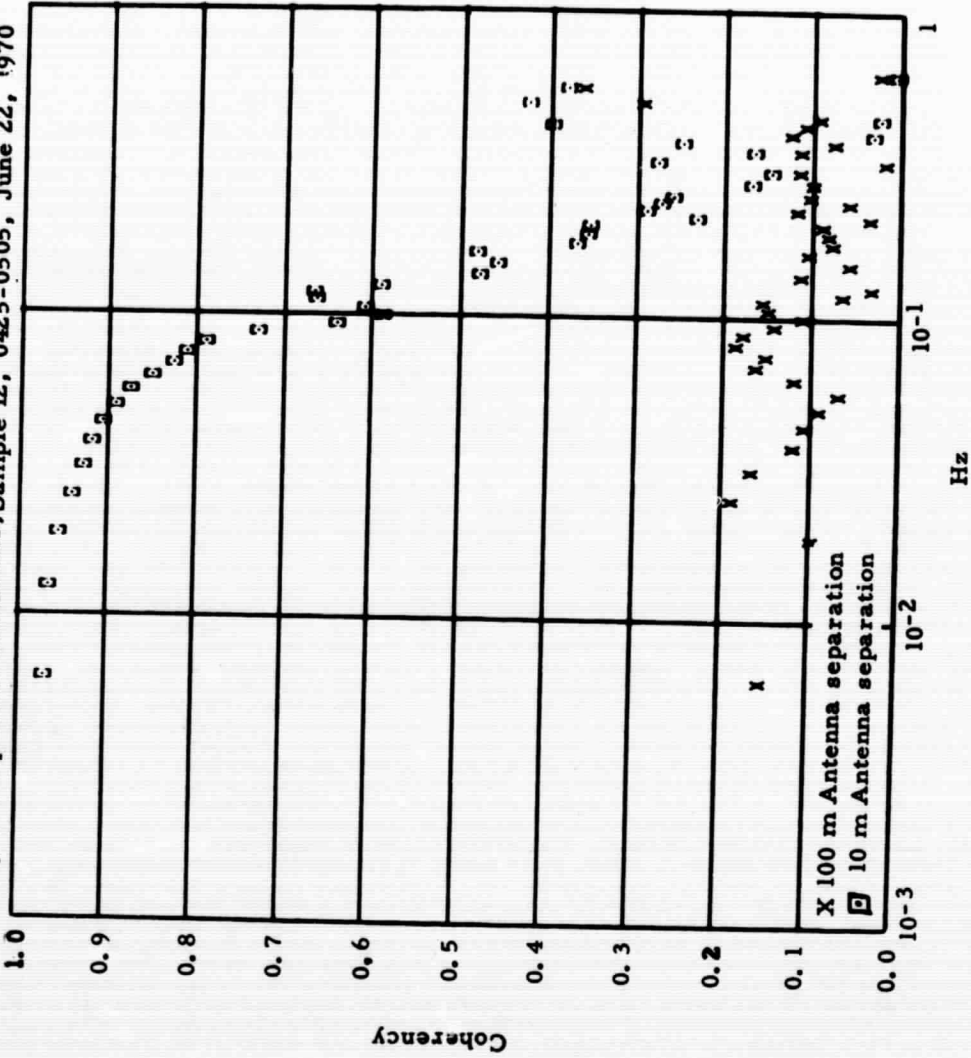Coherency of Amplitude Variations, Sample 12, 0425-0505, June 22, 1970

Fig. 15

OCCULTATION EXPERIMENT

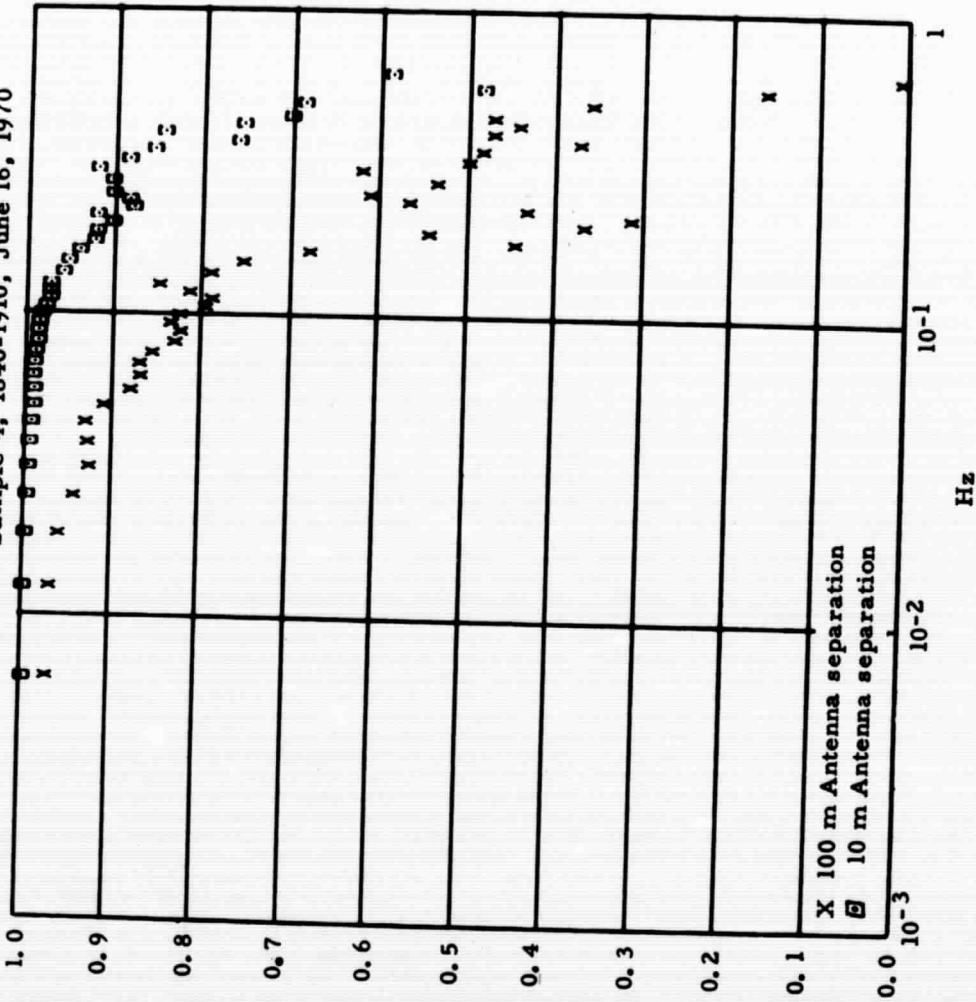Coherency of Phase Variations, Sample 4, 1840-1910, June 16, 1970

X 100 m Antenna separation
⊟ 10 m Antenna separation

Hz

Fig. 16

Appendix I

Estimation of the refractive index structure parameter C_n^2

One of the objectives of this experiment was to obtain estimates of the atmospheric refractive index structure parameter C_n^2 along the propagation path in conjunction with the phase and amplitude variability measurements. This was accomplished during 10 of the sample periods in which flight pattern type I was flown. (See sketch in Fig. 4.)

Three estimates of C_n^2 were obtained from the level portion of each flight. Each C_n^2 value was computed from a 3-minute segment taken from the continuous magnetic tape record of refractive index variations. Briefly, the steps in the computation were as follows:

1.   The continuous analog tape record was digitized at the rate of 800 points per second.

2.   The power spectrum was computed over the frequency range 0.04 to 40 Hz, which is the pass band of the high-resolution output of the refractometer. The high frequency end of the spectrum was contaminated by intrusion of the system noise spectrum, so that the effective frequency range of the analysis was from 0.04 Hz to an upper limit that varied from about 0.2 to 20 Hz, depending on the signal-to-noise ratio of the data.

3.   The structure function, $D(r)$, was computed from each power spectrum and the corresponding aircraft airspeed data for r (spatial separation of refractive index points) ranging from 10 m to 1 km.

4. C_n^2 was then computed as the slope of a linear regression of $D(r)$ on $r^{2/3}$, in line with the defining equation:

$$D(r) = C_n^2 r^{2/3} .$$

The C_n^2 values are tabulated below. The data segments from each flight are identified as "A", "B", or "C". Segments "A" were taken near the northern, or Haleakala, end of the path; segments "B" were taken near the middle of the path, and segments "C" were taken near the southern, or Mauna Loa, end.

Flight No.	Segment		
	$\underline{A}$	$\underline{B}$	$\underline{C}$
1	$2.74 \times 10^{-15} \, m^{-2/3}$	$1.14 \times 10^{-15} \, m^{-2/3}$	$2.76 \times 10^{-15} \, m^{-2/3}$
2	1.08×10^{-15}	3.21×10^{-15}	1.90×10^{-14}
3	3.24×10^{-16}	5.45×10^{-15}	1.59×10^{-15}
4	2.82×10^{-15}	8.57×10^{-16}	2.29×10^{-16}
5	--	1.37×10^{-15}	4.81×10^{-15}
7	6.67×10^{-15}	2.78×10^{-14}	1.11×10^{-13}
14	7.41×10^{-16}	4.60×10^{-15}	1.75×10^{-14}
15	1.39×10^{-13}	1.00×10^{-14}	7.27×10^{-16}
17	2.27×10^{-14}	9.66×10^{-15}	4.52×10^{-15}
18	7.04×10^{-14}	4.74×10^{-14}	7.82×10^{-14}

APPENDIX IV

Method of Measuring Phase, Phase Difference,
and Amplitude

The phase measurements were made using a technique developed
by Thompson and Vetter [1] and shown in Fig. 1.

At the left terminal, a stable microwave signal is generated at
frequency f. This signal is fed to the antenna through a circulator
which also couples a small amount of power to the mixer to serve as
the local oscillator to heterodyne the small signal received from the
opposite teminal.

At the right terminal, a second microwave signal is generated and
phase locked below the frequency of the small signal received from the
left terminal by an amount δ_1. Most of this power is transmitted
back over the path with a small fraction being used as local oscillator
for the right-hand mixer.

The two mixers thus produce signals with frequencies and phases
respectively (left and right)

$$\delta_1 , \left[\phi_0 - \phi_1 - \frac{n_1 L}{c} (f - \delta_1) \right] ,$$

$$\delta_1 , \left[\phi_0 - \phi_1 + \frac{n_1 L f}{c} \right] ,$$

where n_1 is the average refractive index along path 1 (length L), and
ϕ_0 and ϕ_1 are reference phases for the two microwave signals.

The left-hand IF is telemetered to the right terminal where its phase is

$$\phi_0 - \phi_1 - \frac{n_1 L}{c}(f - \delta_1) + \frac{n_1 L}{c}\delta_1 \quad .$$

This signal and the local IF are compared in a phase recorder and give an output of

$$\alpha_1 = \frac{2 n_1 L f}{c} - \frac{2 n_1 L \delta_1}{c} \quad .$$

Since

$$\delta \approx f \times 10^{-5} \, , \quad \frac{\alpha_1}{2} \doteq \theta_1 \equiv \frac{n_1 L f}{c} \quad ,$$

the phase shift over path 1.

This process is repeated at antennas 2 and 3 using different frequency offsets between the right-hand signal and the left-hand signal to provide different IF's. Each pair of IF's is processed the same way as described above to obtain the three path phase records, θ_1, θ_2, and θ_3, separately.

To minimize the errors in determining the phase differences between paths, the six IF signals (3 pairs) are combined as shown in Fig. 2.

Lower side band mixers are used to combine X with Y and X' with Y'. The result is two second IF's having frequency phases (with $\delta_2 > \delta_1$),

$$D: (\delta_2 - \delta_1), \; \left[\phi_1 - \phi_2 - \frac{Lf}{c}(n_1 - n_2) \right]$$

$$D': (\delta_2 - \delta_1), \; \left[\phi_1 - \phi_2 + \frac{Lf}{c}(n_1 - n_2) - \frac{L}{c}(n_1 \delta_1 - n_2 \delta_2) \right] \; .$$

Comparing these signals in a phase recorder gives

$$\beta_{12} = \frac{2Lf}{c}(n_1 - n_2) + \frac{L}{c}(n_2 \delta_2 - n_1 \delta_1) \; .$$

Since $n_2 \overset{\bullet}{=} n_1$ and $(\delta_2 - \delta_1) << f$, we have

$$\frac{\beta_{12}}{2} \overset{\bullet}{=} (\theta_1 - \theta_2) \equiv \Delta\theta_{12} \; .$$

By repeating this process with X, Z and X', Z', we obtain a record of $\Delta\theta_{13}$.

Amplitudes for all paths are recorded in terms of the IF signals at the right-hand terminals using commercial amplitude detectors.

Reference

[1] Thompson, M. C., Jr., and M. J. Vetter (1958), "Single path measuring system for three-centimeter radio waves," Rev. Sci. Instr. 29, No. 2, 148-150.
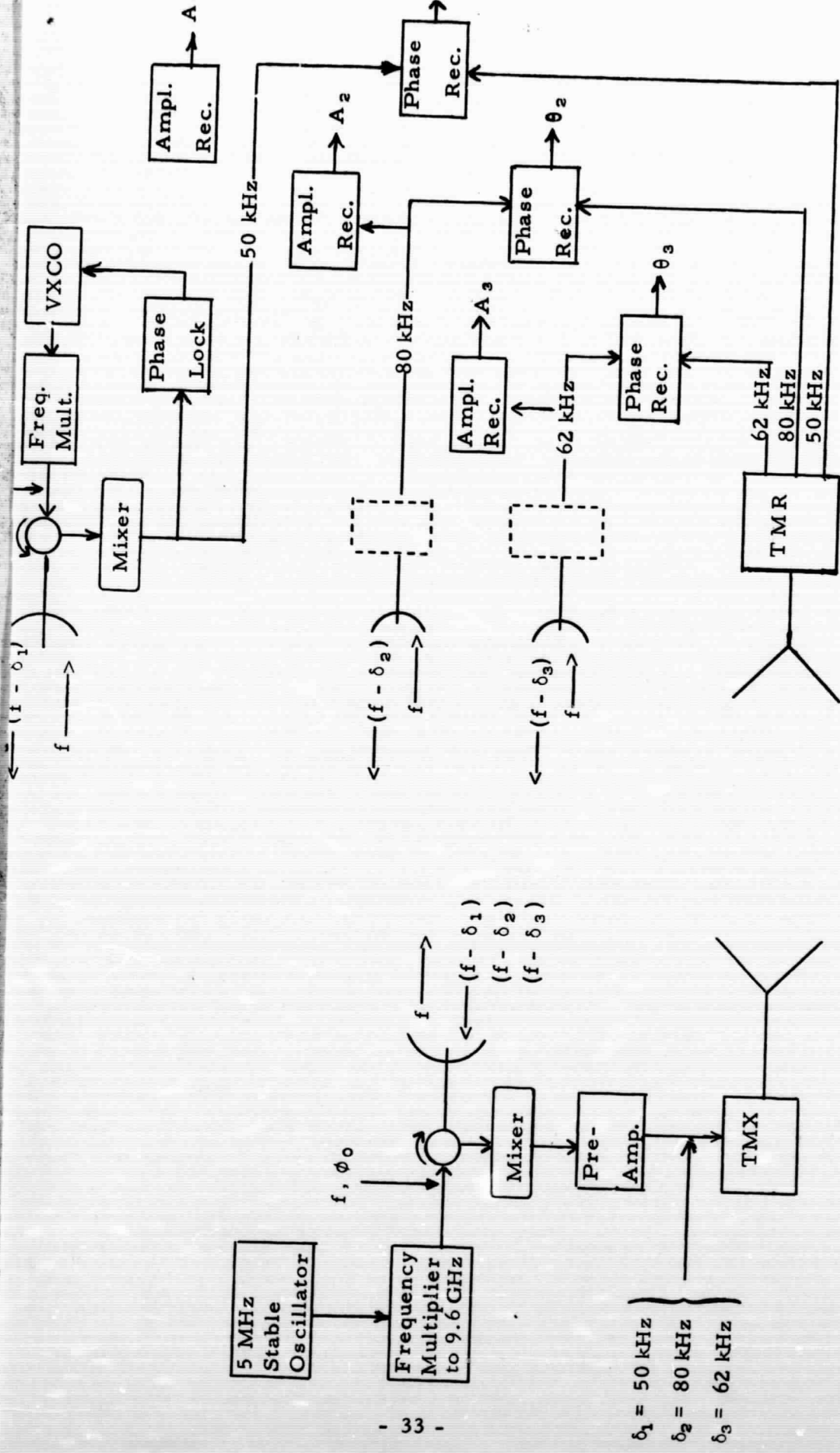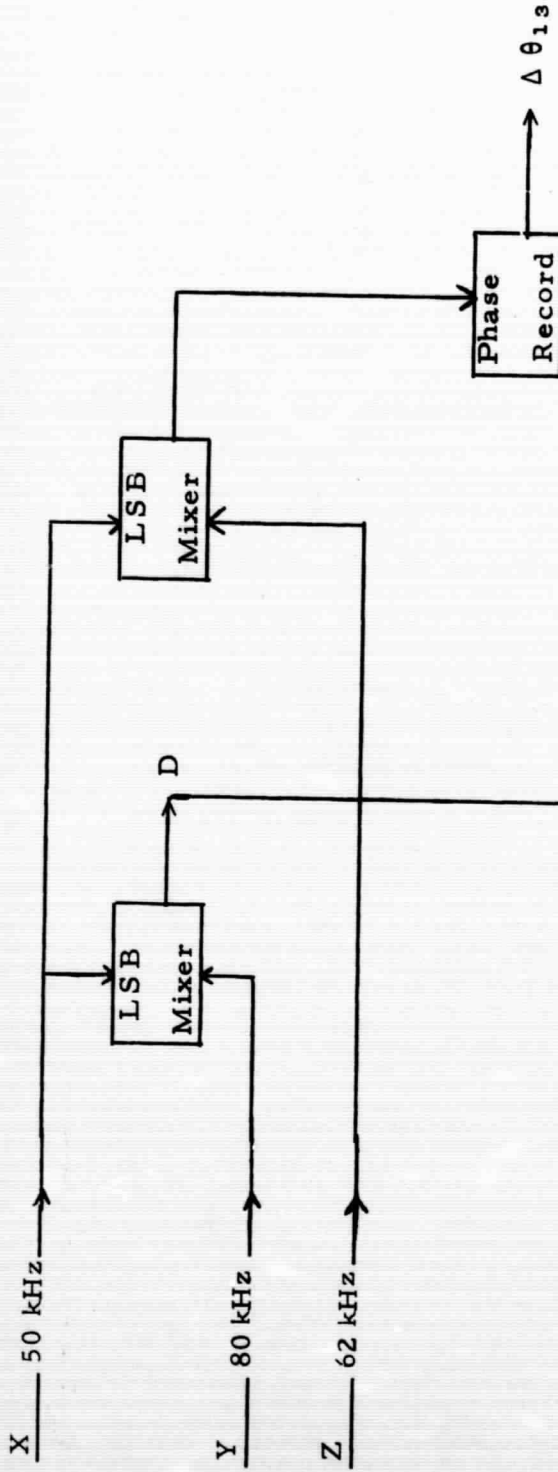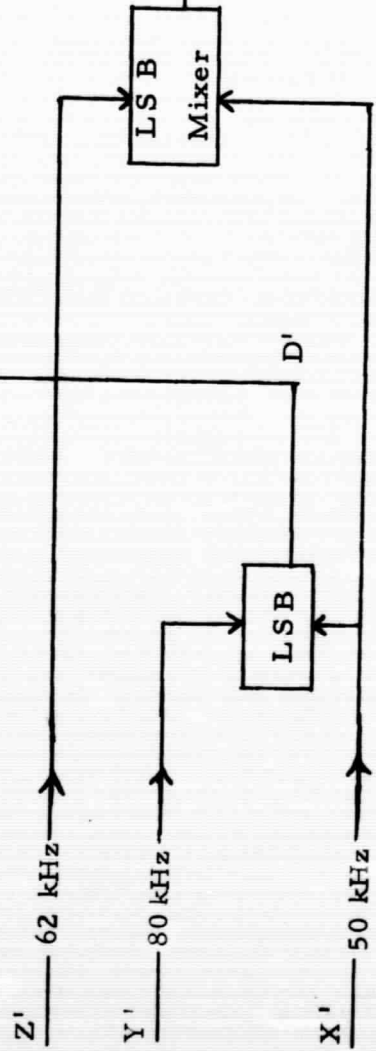
Figure 1. Phase and amplitude measurement system.

Figure 2. Phase-difference measurement system.